Experimental characterization of cyclic behaviour of pure lead: temperature sensitivity and strain-rate effects

[1,*]E. Solfiti, [2]L. M. Viespoli, [2]M. A. Lervåg, [2]T. A. Kristensen, [3]R. Esposito, [3]M. Calviani, [3]R. Franqueira Ximenes, [1,4]F. Berto, [1,2]A. Alvaro

[1]*Department of Mechanical and Industrial Engineering, Norwegian University of Science and Technology, Trondheim, 7491, Norway*

[2]*Department of Material and Nanotechnology, SINTEF Industry, Trondheim, Norway*

[3]*European Laboratory for Particle Physics (CERN), 1211 Geneva 23, Switzerland*

[4]*Department of Chemical Engineering Materials Environment, Sapienza University of Rome, Rome, Italy*

Abstract

Proton beam pulses with an energy of 20 GeV/*c* collide with a pure-lead based target installed in the neutron Time-Of-Flight facility (n_TOF) at the European Laboratory for Particle Physics (CERN). The interaction between the proton beam and lead produces neutrons via *spallation* mechanism and results in a rapid temperature increase and propagation of stress waves. To evaluate the material response in such challenging conditions, a reliable thermo-mechanical characterization is necessary for the calibration of an appropriate constitutive model for pure lead that is valid under cyclic plasticity and high temperature. In this work, the experimental bases for the development of such constitutive material description are lied. Starting with metallurgical characterization, the typical grain size of the material was initially investigated as well as any variations in the metallurgical features. The grains appeared to have an equivalent size ranging from 2 to 6 mm. Then, static tensile tests were conducted at room temperature and different strain-rates from 10^{-1} to 10^{-4} s^{-1}. The obtained results were crucial for optimizing the specimen geometry and test setup for the subsequent cyclic tests. Tension-compression cyclic tests were performed at different strain amplitudes from 0.1 to 1.5%, and at three different temperatures (room temperature, 90°C and 150°C). The strain amplitudes were controlled by an extensometer and the strain field evolution during the test was recorded by means of 2D DIC.

Keywords

Pure lead; creep; cyclic deformation; Time-Of-Flight facility target.

1. Introduction

The characterization of cyclic behaviour of pure lead presented in this paper has been carried out to better understand the thermo-mechanical behaviour of the neutron spallation target installed in the neutron Time-Of-Flight facility (n_TOF) at the European Laboratory for Particle Physics (CERN). The n_TOF facility is a neutron source capable of providing high-intensity neutron pulses for neutron cross-section measurements based on the time-of-flight method (Gunsing et al. 2017). An overview of the facility is shown in Fig. 1 (Esposito, Calviani et al. 2021). Proton beam pulses with an energy of 20 GeV/*c* are extracted from the Proton Synchrotron accelerator ring at CERN and collide with a pure-lead based target. The interaction between beam and target produces neutrons via *spallation* mechanism

[*]Corresponding author. *E-mail address:* emanuele.solfiti@ntnu.no

(Colonna, Gunsing, and Käppeler 2018). On average, each proton produces 300 neutrons (Mingrone 2016). The neutrons travel toward two experimental areas where samples and detectors for neutron-induced reaction measurements are installed. The measurements performed at n_TOF are important for a wide range of applications in nuclear physics, nuclear technology, astrophysics, and medicine (Chiaveri et al. 2020).

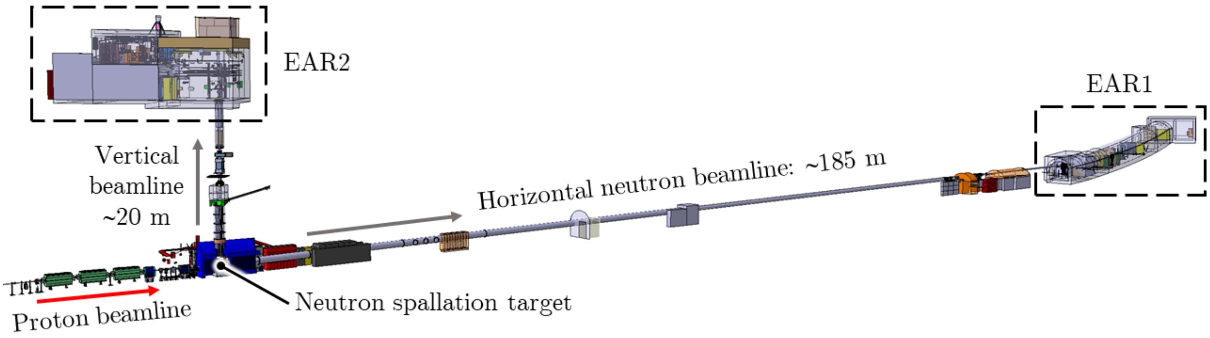

Fig. 1: Overview of the n_TOF facility at CERN. A 20-GeV/c proton beam impacts a pure-lead target providing neutrons via spallation mechanism to the two experimental areas EAR1 and EAR2 (Esposito, Calviani et al. 2021).

The definition of a reliable design for the neutron spallation target requires a good understanding and a reliable characterization of its thermo-mechanical response when impacted by proton beam. Each proton pulse can have up to 10^{13} protons at 20 GeV/c and impacts the target with a minimum period of 1.2 s. During the interaction, about half of the energy of a single proton pulse (up to 32 kJ) dissipates in form of heat in the target in only 25 ns. This provokes, inside the pure-lead target, a rapid temperature increase and consequent thermal expansion that leads to violent dynamic phenomena with propagation of stress waves. The temperature spike is followed by fast thermal diffusion and rapid cooling. The high-purity lead in the target works in the elastic-plastic regime when subjected to the stress field due to the evolution of thermal gradients and propagation of stress waves. The choice of high purity lead (>99.98%) as spallation material is dictated by physics requirements related to the neutron production. The periodic character of the proton beam impacts, the thermal cycles, and the passage of stress waves induce a cyclic loading on pure lead in the elastic-plastic regime. The evolution of temperature and stress in the target can be estimated by Finite Element Model (FEM) simulations, for which an appropriate constitutive model of pure lead valid in cyclic plasticity conditions is required. To define a reliable constitutive model, experimental stress-strain curves under cyclic loading are needed. However, cyclic stress-strain curves of pure lead for different values of strain-range amplitude, temperature, and strain-rate are not available in the literature.

Pure lead has a melting point of 600 K, which means that diffusional mechanisms are active even at room temperature. The material is therefore prone to recrystallization phenomena already at moderate temperatures and will permanently deform due to creep mechanisms when subjected to shear stress during application. The good formability, the resistance of lead to external agents, and its high density, have made this the material of choice for specific applications in various fields born, or highly developed, in the last century. Lead is in fact broadly used as water barrier for subsea high voltage power cables, as solder material in the electronics industry, and as radiation (photon) shielding in the nuclear and medical industries.

The study of the phenomenon of creep is of utmost importance to enable an accurate description and prediction of the mechanical response of this material to monotonic and cyclic external loads and of the consequent damage mechanisms. The term creep refers to the permanent, time-dependent deformation of a metal that occurs when sufficient temperature and stress are present. Depending on the temperature and stress (or strain rate) levels, the phenomenon might be dominated by diffusion or dislocation glide and climb. Under cyclic loading, the weakening of grain boundaries and the increased amount of plastic deformation may reduce the number of loading cycles required to initiate damage, which generally occurs at the grain boundaries for elevated temperatures, and then propagates at faster rate than in the absence of creep. To assess the structural integrity of components under creep deformation and damage, it is therefore necessary to account for the impact of this phenomenon with opportune modelling tools (Kassner 2015; Takahashi 2009; Viespoli and Berto 2019; Wu, Yang, and Zhao 2020).

In addition, the creep response impacts the apparent elastic modulus of the material and the flow stress reached to impose a certain strain rate (Lall et al. 2016; Motalab et al. 2012; Pang et al. 1998).

It is known that grain size affects the response of a polycrystalline metal lattice in presence of diffusional creep, with bigger grains reducing the detrimental effect of grain boundaries with respect to creep induced damage (Kassner and Pérez-Prado 2000; Mohamed and Langdon 1974).

The strength of lead-based alloys has been investigated in the cable industry to estimate the lifetime of the lead sheathing necessary to ensure electrical insulation from water impregnation; characterizing the behaviour of lead alloys under both monotonic and cyclic loads is critical for this purpose. However, being these studies strongly tied to a specific field/application, the available research on the subject in terms of alloys investigated, experimental procedures, and characterization techniques is limited and largely outdated, dating back several decades (Anelli, Donazzi, and Lawson 1988; Dollins and Betzer 1956; Feltham 1956; Harvard 1972; Linul et al. 2017; Moore and Alleman 1932; Sahota and Riddington 2000). In recent years, however, with the growing need for interconnection of national electrical grids, renewed interest in the energy sector has led to the development of new studies focusing on the mechanical response of lead accounting for factors such as microstructure, production defects, and loading type. These studies encompass investigations performed at the microstructural, macrostructural, and full-component levels (Johanson et al. 2018, 2019; Moreno et al. 2021; Viespoli, Johanson, Alvaro, Nyhus, and Berto 2019; Viespoli, Johanson, Alvaro, Nyhus, Sommacal, et al. 2019; Viespoli et al. 2019; Viespoli et al. 2020, 2021; Wan et al. 2020).

2. Materials and methods

2.1. Materials

The material investigated in this study is high-purity lead (purity level >99.99%) provided by Metall-Technik Halsbrücke GmbH & Co. (MTH) in the form of four cast blocks of 300 mm × 300 mm × 50mm each (see Fig. 2). Based on the authors' previous experience with lead alloys (Johanson et al. 2018, 2019; Moreno et al. 2021; Viespoli, Johanson, Alvaro, Nyhus, and Berto 2019; Viespoli, Johanson, Alvaro, Nyhus, Sommacal, et al. 2019; Viespoli et al. 2019; Viespoli et al. 2020, 2021; Wan et al. 2020), and due to the low melting temperature and yield point of lead, its microstructure is prone to changes even under small loads and moderate temperature variations. This, in turn, may affect both the material monotonic and cyclic response. To evaluate the suitability of the material preparation and machining procedure, metallurgical investigation trials were performed both on as-received and heat-treated (150°C for 2 hours) specimens.

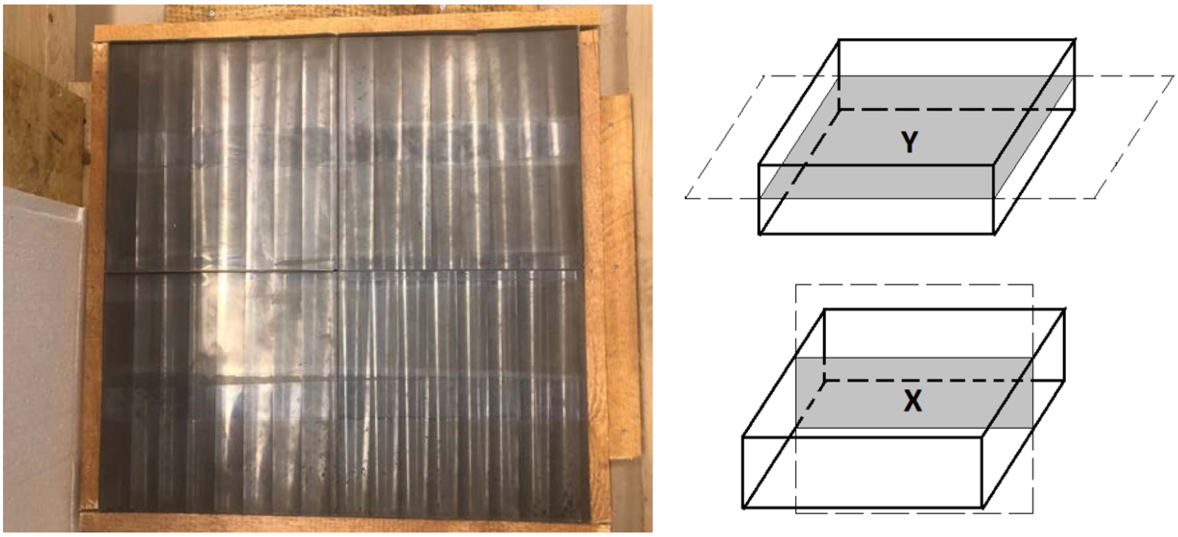

Fig. 2: Left: as-received cast blocks of pure lead; right: schematics indicating the planes of reference for the microstructural characterization.

Fig. 3 presents the results of these trials: the as-received specimen featured bigger grains than those observed on the heat treated one, as expected due to the activation of the recrystallization process induced by the heat treatment. This indicates that the preparation procedure was suitable for revealing the real metallurgical structure of lead. Additionally, the lack of grain size variation along the specimen's edges suggests that also the machining of the specimens via Electron Discharge Machining (EDM) does not significantly affect the microstructure.

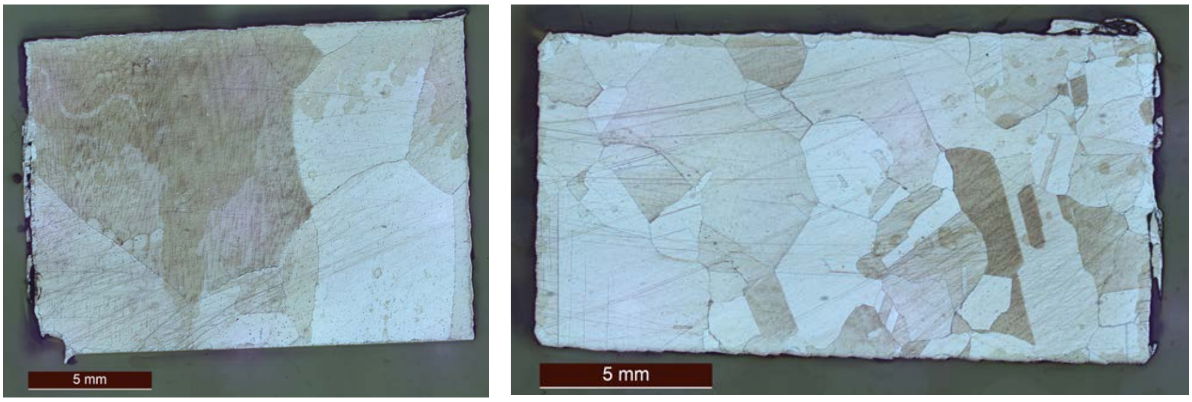

(a) (b)

Fig. 3: Results of metallurgical investigation trials performed on: a) as-received specimen; b) heat-treated specimen.

Once the suitability of the specimen preparation and machining procedure was confirmed, the cast blocks of pure lead were examined in different orientations and positions, as shown in Fig. 2. The macrographs resulting from examining the as-received block in the two different orientations shown in Fig. 2 (from top of the block and side of the block) are reported in Fig. 4. No significant difference in grain size or morphology can be observed with respect to the orientations. However, the edges of the two specimens revealed smaller grains, likely due to the conditions the material was exposed to during transportation and storage.

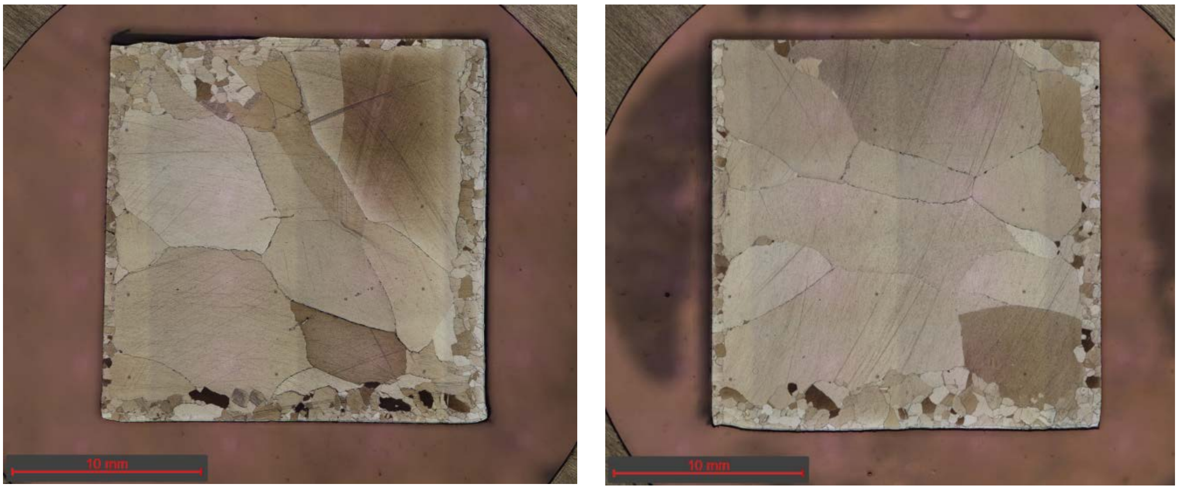

(a) (b)

Fig. 4: Metallurgy of as-received cast blocks of pure lead performed on: a) orientation X; b) orientation Y (refer to Fig. 2).

2.2. Mechanical testing

Even though the main goal of the experimental campaign is to characterize the material's cyclic behaviour under different temperature and strain rate conditions, a first round of monotonic tensile testing was conducted to gain valuable insights regarding suitable dimensions for the test specimen design.

Monotonic tensile testing

Since no standards or common practice are available in literature regarding mechanical testing of pure lead, a first exploratory round of static tensile tests was performed using the geometry shown in Fig. 5(a) to determine the best setup parameters. The tests were conducted at room temperature (20°C) under displacement control and the strain-rate was varied from 10^{-1} to 10^{-4} s^{-1}.

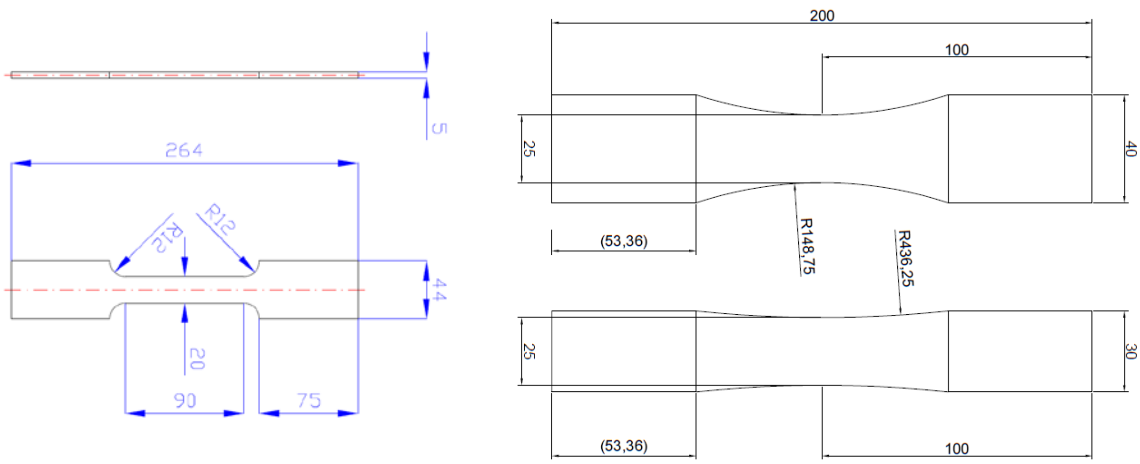

(a) (b)

Fig. 5: Specimen geometries used for mechanical testing (dimensions in mm): (a) thin specimen according to NS-EN-ISO 6892-1:2016 and (b) square section specimen adopted for cyclic testing.

The displacement was also measured by DIC (Digital Image Correlation) and compared with the machine's stroke output (see Fig. 6). Based on the results of the metallurgical characterization, which showed a grain size ranging from 2 to 5 mm and the observation of the "orange peeling effect" from the tensile testing performed on the specimen shown in Fig. 5(a), it was deemed necessary to use a new specimen geometry to ensure the validity of the results. Fig. 5(b) shows the design and the relevant dimensions of the specimen used for the cyclic testing of the material.

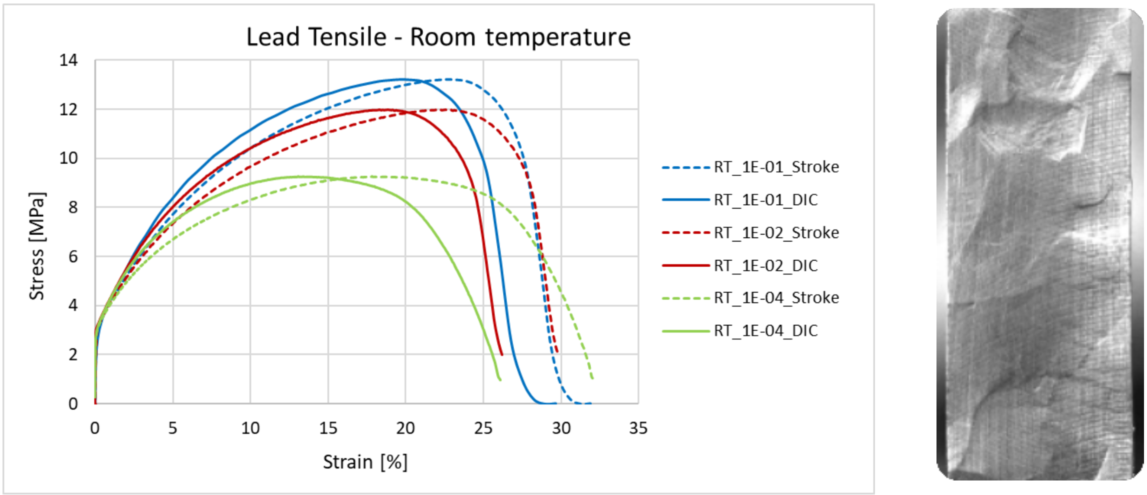

Fig. 6: Stress-strain curves of pure lead at room temperature and different strain rates obtained by measuring both machine stroke and DIC. "Orange peel" effect due to the grain "protrusion" from the specimen surface is also clearly visible on the longitudinal view of the specimen.

Cyclic testing

All the mechanical cyclic tests were performed in a 25-kN servo-hydraulic test machine from Dartec under strain control by using a 25-mm MTS extensometer attached directly to the specimen's surface. Cyclic mechanical testing of pure lead presents peculiar challenges, particularly when it comes to gripping: due to its low melting temperature, high ductility and creep tendency, the material is strongly prone to slip when gripped and such behaviour is accentuated as the testing temperature increases. To address this, special grips were designed for the cyclic testing. The grips were equipped with four M12 bolts per side, and a set of Belleville washers was compressed by each bolt to ensure constant gripping load even in case of a significant amount of material relaxation. In addition, grooves oriented perpendicular to the loading direction were dug on the inner grip surface to increase friction between the grips' inner surface and the specimen gripping area. Test set-up, including pictures of the grips, are shown in Fig. 7.

The extensometer provided real-time feedback to the test machine so that a constant strain rate could be maintained and the target value for a given maximum strain amplitude could be reliably reached. Additionally, the sine wave frequency was automatically adjusted by the machine based on the extensometer recording to maintain the target strain rate for different imposed strain ranges. Furthermore, an in-house DIC system with a 5 MPixel Prosilica camera was used to obtain second feedback on the strain development, both in the gauge between the extensometer knives and at other possible locations of interest on the specimens' surface.

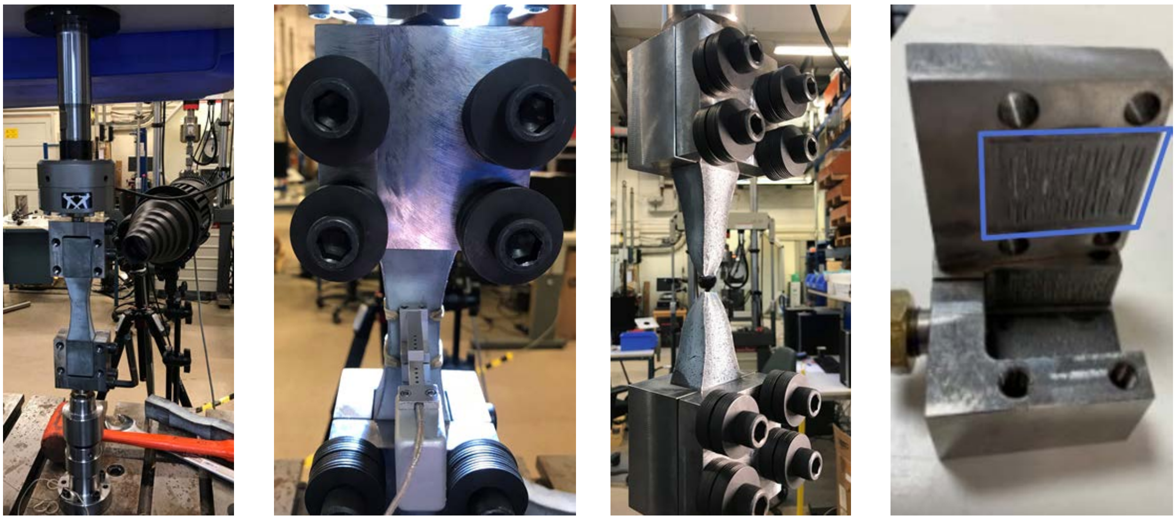

(a) (b) (c) (d)

Fig. 7: (a) Overview of test set-up, including DIC camera; (b) and (c) close-up on the specimen with extensometer and on the gripping system and specimen after failure; (d) picture showing grooves engraved inside the grips for an improved gripping.

Cyclic testing was performed at various fixed maximum strain amplitudes imposed in both an increasing and decreasing stepwise sequence and for three different temperatures, as summarized in Table 1. Thirty cycles were imposed for each $\Delta\varepsilon$ level. Additionally, a final relaxation stage was implemented for tests 2, 3, 4, 5, 1T, 2T, 3T and 4T, whose duration is also reported in Table 1.

Table 1. Test matrix for cyclic tests

Test ID	1	2	3	4	5	6	1T	2T	3T	4T
Strain-rate [s^{-1}]	10^{-2}	10^{-3}	10^{-1}	10^{-1}	10^{-2}	10^{-1}	10^{-2}	10^{-2}	10^{-1}	10^{-1}
Temperature [°C]	20	20	20	20	20	20	90	150	90	150
Strain amplitudes $\Delta\varepsilon/2$ [%]	± 0.1	± 0.1	-	-	± 0.1	± 1.5	± 0.1	± 0.1	-	-
	± 0.2	± 0.2	± 0.2	-	± 0.2	± 1	± 0.2	± 0.2	-	-
	± 0.5	± 0.5	± 0.5	± 0.5	± 0.5	± 0.5	± 0.5	± 0.5	± 0.5	± 0.5
	± 1	± 1	± 1	± 1	± 1	± 0.2	± 1	± 1	± 1	± 1
	± 1.5	± 1.5	± 1.5	± 1.5	± 1.5	± 0.1	± 1.5	± 1.5	± 1.5	± 1.5
Holding time [hh:mm:ss]	-	13:58:00	00:25:23	14:13:52	15:06:00	-	00:43:49	00:21:00	00:21:12	00:19:23

3. Experimental results

The typical set of data captured by the extensometer in each cyclic test is shown in Fig. 8. Fig. 8a illustrates an example of nominal strain - time history imposed by the machine on the length of specimen comprised between the two extensometer's blades. The time derivative of such signal yields the nominal strain rate imposed on the specimen volume, which is plotted against time in Fig. 8b. Despite the noise, the target nominal strain rate value (10^{-2} s^{-1} in the case shown in Fig. 8) is clearly obtained and maintained throughout the entire test. The strain rate oscillates from positive to negative according to the machine's crosshead direction of motion. Figure 8c finally shows the corresponding stress-strain curve as recorded by the system. Several effects related to the ductile behaviour of lead can be observed in the hysteresis curves: as the strain amplitude increases, the plastic component of deformation gradually becomes more relevant and shows evidence of Bauschinger effect. At lower strain amplitudes ($\Delta\varepsilon < 1\%$), a degree of strain hardening is detected. The magnitude of cyclic hardening decreases for each subsequent cycle until reaching saturation within the 30 cycles imposed for each strain level. The saturation of cyclic hardening is reached for a stress value that increases with the strain amplitude. For $\Delta\varepsilon \geq 1\%$, this effect reaches a plateau, and the peak stress does not increase further with increasing strain amplitude.

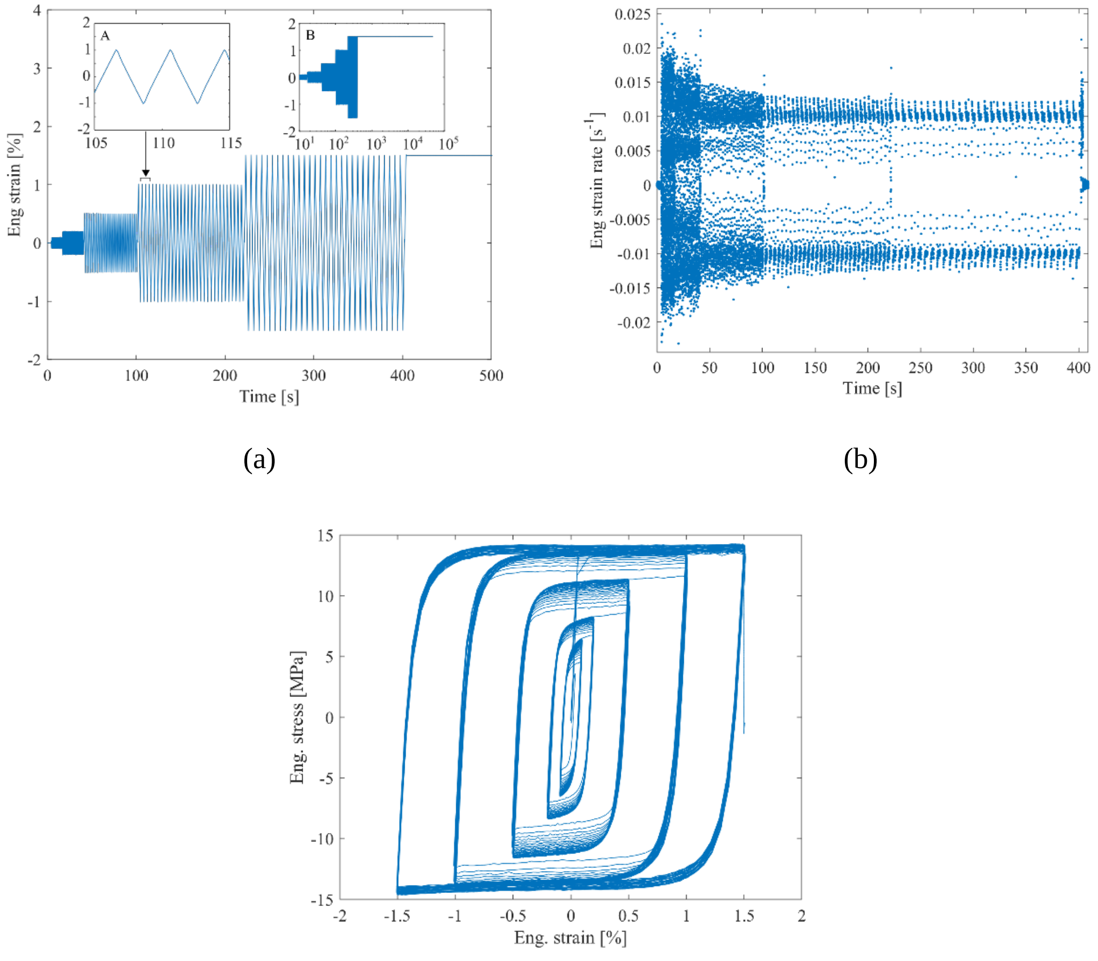

(c)

Fig. 8. Output curves for test 5:(a) extensometer strain vs time history: inset A shows a detailed view of 3 cycles with $\Delta\varepsilon/2$ = 1%, and inset B shows the whole history in semi-log coordinates including the final relaxation stage; (b) engineering strain rate vs time; (c) engineering stress vs engineering strain.

In addition, the recorded pictures of the specimen surface were analysed with 2D DIC to gain greater insight into the local strain variations during the test. Strain histories were extracted from virtual extensometers of different lengths passing both inside and across the gauge length (Figure 9a-b). The strain evolution from the three shortest extensometers shows a positive drift of the average deformation, i.e., an elongation of the central section of the sample. Additionally, the strain range in this section appears to be greater than the one measured by the extensometer, while the strain range obtained through DIC and measured by the longest vectors is slightly smaller. The drift in the mean stress levels obtained by the DIC measurements is likely due to progressive bending of the specimen caused by inhomogeneous material flow during the cyclic deformation. Such inhomogeneities in the strain distribution along the specimen's longitudinal coordinate shall be accounted for in post-processing the results for material model calibration.

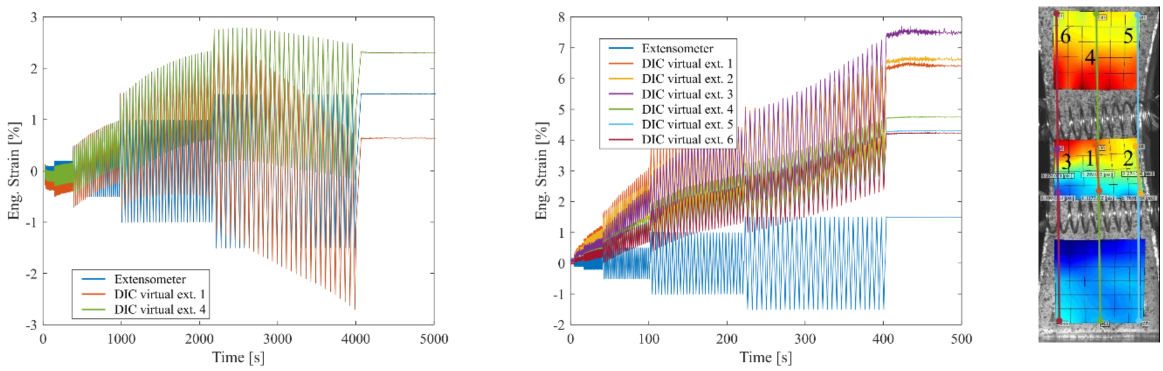

(a) (b) (c)

Fig. 9: DIC and extensometer strains: (a) test 2 and (b) test 1T. (c) The strains were calculated from the length variation of six vectors placed longitudinally along the specimen surface. Short vectors 1,2, and 3 measured the displacement within the gauge length, long vectors 4,5, and 6 measured the largest displacement available from the images. The areas occupied by the extensometer were not included in the analysis.

Fig. 10a-b shows some examples of the hysteresis cycles obtained at fixed strain rate and varying temperatures. For a given temperature, increasing the nominal strain rate from 10^{-2} to 10^{-1} s^{-1} always results in a stress level increase, at least within this strain rate range. However, it must be pointed out that for the tests at room temperature, creep deformation mechanisms are active but less relevant than at higher temperature. Observing Fig. 10a-b we can see how the stress change from one strain rate to the other is relatively greater at the higher temperature levels. Analogously, the impact of testing temperature is more prominent at lower strain rates: a single cycle allows more time for creep deformation mechanisms to act, mechanisms that are subjected to even greater activation as the temperature is raised. In Fig. 10c the peak stresses were reported against the number of cycles. Clearly, for all the tests with increasing $\Delta\varepsilon$, the peak stresses reached a stabilized value before 15 – 20 cycles. Fig. 10d, with the help of Fig. 10c (dashed black line), shows the hysteresis cycles for a test in which the stepwise application of the target strain amplitude levels is applied in a decreasing order (test 6). While the initial loading cycles clearly show cyclic hardening, the convergence to a stabilized stress is approached by cyclic softening at every reduction of strain amplitude. The latter appears also faster than the convergence under increasing strain amplitudes and cyclic hardening.

In Figure 11, the stress is reported against the relaxation time where the strain is held constant at the maximum value of the last cycle. The time needed to recover the stress at 20% and 10% of the initial maximum load are reported in the side table of Figure 11. In general, tests performed at room temperature show a much slower recovery than tests executed at high temperatures. However, at least in the first stages of recovery, a faster decrease is observed for tests at higher strain-rates. Note, for example, that in test 5 (10^{-1} s^{-1}), 80% of the initial load is recovered in 22.14 s, which is much faster than in tests 2 and 4. However, it then experiences a milder descent and slows down until reaching 10% of the maximum load in 370 s. Similarly, the higher strain-rate tests 3T and 4T recover faster down to 20% of the maximum load but then markedly slow down the recovery.

A non-monotonic regime appears when the stress is almost recovered, especially at high temperature. The stress also decreases below zero, probably as a result of residual stress from the previous cyclic history.

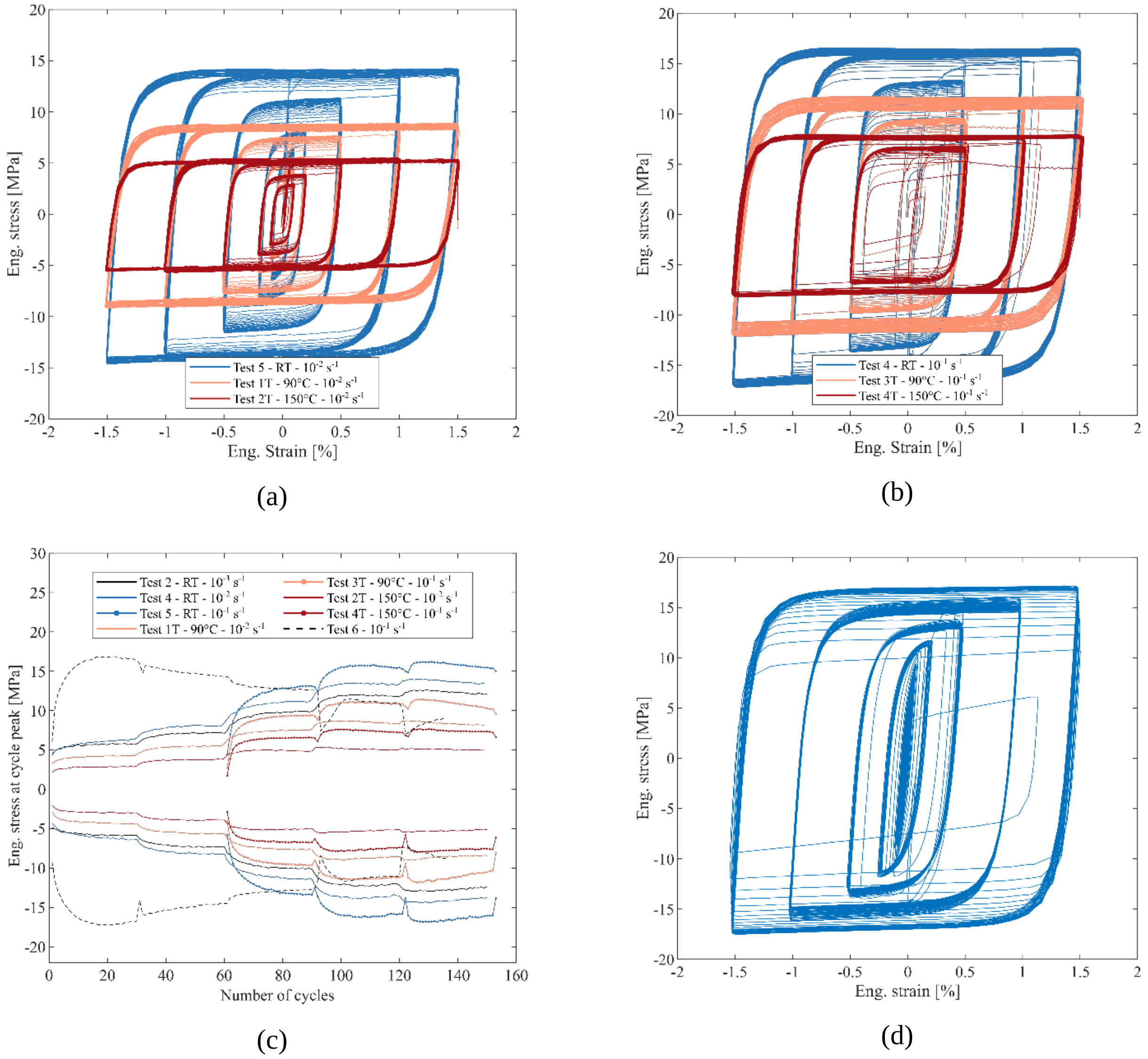

Figure 10. Stress vs extensometer strain curves at room temperature (RT), 90°C, and 150°C. (a) Strain-rate = 10^{-2} s^{-1}. (b) Strain-rate = 10^{-1} s^{-1}. (c) The peak stress at each cycle is reported against number of cycles. The plots of tests 5, 3T, and 4T have been shifted to visually match the strain amplitude levels. (d) Stress vs extensometer strain curves for test 6 with decreasing strain amplitudes.

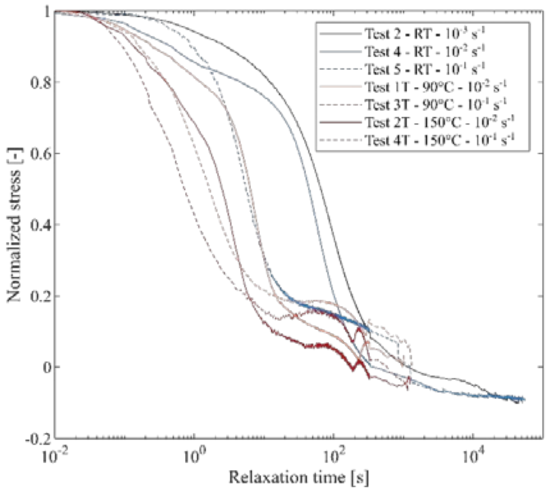

Test id.	Recovery time [s] for 20% of max. load	Recovery time [s] for 10% of max. load
2	181.01	316.812
4	101.27	154.155
5	122.139	370.021
1T	15.071	67.971
3T	12.867	258.78
2T	5.963	12.88
4T	5.166	148.92

Figure 11. Stress relaxation tests. The engineering stress at constant strain is reported against time in semi-logarithmic coordinates. The curves have been shifted so that the zero-time is immediately following the last cycle. On the side, the values of recovery time at specific load levels extracted from the plot.

Conclusion

The present work is focused on the characterization of the mechanical response of cast high-purity lead under cyclic loading at various temperatures and strain rates. The main conclusions can be summarized as follows:

- The initial metallographic investigation revealed that the grains of the as-received material appear to have an equivalent size ranging from 2 to 6 mm. Due to the large grain size observed and the dimension of the typical cross-section used in the analysis, it is not possible to provide a reliable quantitative estimate. No grain size directional dependency emerged with respect to the section plane,
- The sample subjected to heat treatment, that is exposed to 150°C for 2 hours, exhibited a reduction in the average grain size, due to recrystallization, when compared to the as-received sample,
- The preliminary series of tensile tests performed on dog-bone specimens with a gauge cross section of 20×5 mm^2 showed a significant reduction in ultimate stress as the testing strain rate decreased. However, the strong influence of the free surface on the given material, visualized by the "orange peel" effect, demonstrated the unreliability of the initial specimens’ design and leaded to maximize the cross-section for the subsequent cyclic characterization,
- Cyclic tests were performed imposing a sequence of strain amplitude levels at three different temperatures i.e., 20°C, 90°C and 150°C, and nominal strain rates between 10^{-3} and 10^{-1} s^{-1}. The strain was controlled through an extensometer and, additionally, the tests were recorded by a DIC system. It was observed that for a given strain amplitude, the stress amplitude is reduced at higher temperature. Such effect is amplified at lower strain rate, most probably because of the longer deformation time allowing for more diffusion and/or dislocation climb (depending on the dominant creep mechanism) to take place. After changing between two strain levels, the hysteresis cycle stabilizes in a few hardening cycles and reaches strain history-independent levels whose magnitude is related to the imposed strain amplitude.

The results obtained in this work will serve as foundation for calibrating appropriate cyclic material models that take into account the impact of cyclic hardening, strain memory, and creep effects (Esposito 2022).

Data availability

Data will be made available on request.

Acknowledgements

The authors acknowledge both Norwegian University of Science and Technology (NTNU) and European Organization for Nuclear Research (CERN) for funding this work.

References

Anelli, P., F. Donazzi, and W. G. Lawson. 1988. 'The Fatigue Life of Lead Alloy E as a Sheathing Material for Submarine Power Cables'. *IEEE Transactions on Power Delivery* 3(1):69–75.

Dollins, Curtis Walter and Cecil E. Betzer. 1956. *Creep, Fracture, and Bending of Lead and Lead Alloy Cable Sheathing*. University of Illinois at Urbana Champaign, College of Engineering ….

Feltham, P. 1956. 'On the Mechanism of High-Temperature Creep in Metals with Special Reference to Polycrystalline Lead'. *Proceedings of the Physical Society. Section B* 69(12):1173.

Harvard, D. G. 1972. 'Fatigue of Lead Cable-Sheathing Alloys'. *Ontario Hydro Research*.

Johanson, Audun, Luigi Mario Viespol, Antonio Alvaro, and Filippo Berto. 2019. 'Small-and Full-Scale Fatigue Testing of Lead Cable Sheathing'. in *The 29th International Ocean and Polar Engineering Conference*. OnePetro.

Johanson, Audun, Luigi Mario Viespoli, Bård Nyhus, Antonio Alvaro, and Filippo Berto. 2018. 'Experimental and Numerical Investigation of Strain Distribution of Notched Lead Fatigue Test Specimen'.

Kassner, M. E. and M. T. Pérez-Prado. 2000. 'Five-Power-Law Creep in Single Phase Metals and Alloys'. *Progress in Materials Science* 45(1):1–102.

Kassner, Michael E. 2015. *Fundamentals of Creep in Metals and Alloys*. Butterworth-Heinemann.

Lall, Pradeep, Di Zhang, Vikas Yadav, and David Locker. 2016. 'High Strain Rate Constitutive Behavior of SAC105 and SAC305 Leadfree Solder during Operation at High Temperature'. *Microelectronics Reliability* 62:4–17.

Linul, E., D. A. Şerban, L. Marsavina, and J. Kovacik. 2017. 'Low-cycle Fatigue Behaviour of Ductile Closed-cell Aluminium Alloy Foams'. *Fatigue & Fracture of Engineering Materials & Structures* 40(4):597–604.

Mohamed, Farghalli A. and Terence G. Langdon. 1974. 'The Transition from Dislocation Climb to Viscous Glide in Creep of Solid Solution Alloys'. *Acta Metallurgica* 22(6):779–88.

Moore, Herbert Fisher and Norville James Alleman. 1932. *The Creep of Lead and Lead Alloys Used for Cable Sheathing, a Report of an Investigation Conducted by the Engineering Experiment Station, University of Illinois in Coöperation with the Utilities Research Commission*. University of Illinois at Urbana Champaign, College of Engineering ….

Moreno, Edgardo, Luigi Mario Viespoli, Audun Johanson, Di Wan, Antonio Alvaro, and Filippo Berto. 2021. 'Effect of Geometrical Irregularities on Fatigue of Lead Sheathing for Submarine High Voltage Power Cable Applications'. *International Journal of Fatigue* 151:106399.

Motalab, Mohammad, Zijie Cai, Jeffrey C. Suhling, and Pradeep Lall. 2012. ‘Determination of Anand Constants for SAC Solders Using Stress-Strain or Creep Data’. Pp. 910–22 in *13th InterSociety Conference on Thermal and Thermomechanical Phenomena in Electronic Systems*. IEEE.

Pang, H. L. J., Y. P. Wang, X. Q. Shi, and Z. P. Wang. 1998. ‘Sensitivity Study of Temperature and Strain Rate Dependent Properties on Solder Joint Fatigue Life’. Pp. 184–89 in *Proceedings of 2nd Electronics Packaging Technology Conference (Cat. No. 98EX235)*. IEEE.

Sahota, M. K. and J. R. Riddington. 2000. ‘Compressive Creep Properties of Lead Alloys’. *Materials & Design* 21(3):159–67.

Takahashi, Yukio. 2009. ‘Creep-Fatigue Interaction: Its Mechanism and Predictability’. in *Asian Pacific Conference for Materials and Mechanics*.

Viespoli, Luigi M, Audun Johanson, Antonio Alvaro, Bård Nyhus, and Filippo Berto. 2019. ‘Strain Controlled Medium Cycle Fatigue of a Notched Pb-Sn-Cd Lead Alloy’. *Engineering Failure Analysis* 104:96–104.

Viespoli, Luigi M, Audun Johanson, Antonio Alvaro, Bård Nyhus, Alberto Sommacal, and Filippo Berto. 2019. ‘Tensile Characterization of a Lead Alloy: Creep Induced Strain Rate Sensitivity’. *Materials Science and Engineering: A* 744:365–75.

Viespoli, Luigi Mario and Filippo Berto. 2019. ‘Rapid Extrapolation of High-temperature Low-cycle Fatigue Curves for a Nickel Superalloy’. *Material Design & Processing Communications* 1(6):e104.

Viespoli, Luigi Mario, Audun Johanson, Antonio Alvaro, Bård Nyhus, and Filippo Berto. 2019. ‘Room Temperature Creep Mechanism of a Pb-Sn-Sb Lead Alloy’. *Procedia Structural Integrity* 18:86–92.

Viespoli, Luigi Mario, Audun Johanson, Antonio Alvaro, Bård Nyhus, and Filippo Berto. 2020. ‘Subsea Power Cable Sheathing: An Investigation of Lead Fatigue Performance’. *Procedia Structural Integrity* 28:344–51.

Viespoli, Luigi Mario, Luigi Panza, Audun Johanson, Antonio Alvaro, Aurelio Somà, and Filippo Berto. 2021. ‘Tape Winding Angle Influence on Subsea Cable Sheathing Fatigue Performance’. *Engineering Structures* 229:111660.

Wan, Di, Luigi Mario Viespoli, Audun Johanson, Anette Brocks Hagen, Filippo Berto, and Antonio Alvaro. 2020. ‘Tensile and Fatigue Behavior of a Pb-Sn-Sb Alloy Investigated via Small-Scale in-Situ Mechanical Testing in SEM’. *Procedia Structural Integrity* 28:648–58.

Wu, Zhiwei, Maosheng Yang, and Kunyu Zhao. 2020. ‘Fatigue Crack Initiation and Propagation at High Temperature of New-Generation Bearing Steel’. *Metals* 11(1):25.

Appendix A

Room temperature tests data

Test 1 (10^{-2} s^{-1}, 20°C)

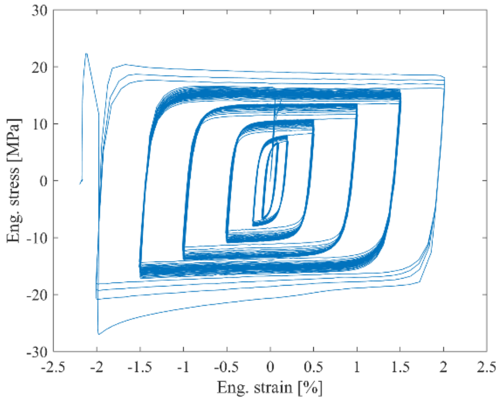

Test 2 (10^{-3} s^{-1}, 20°C)

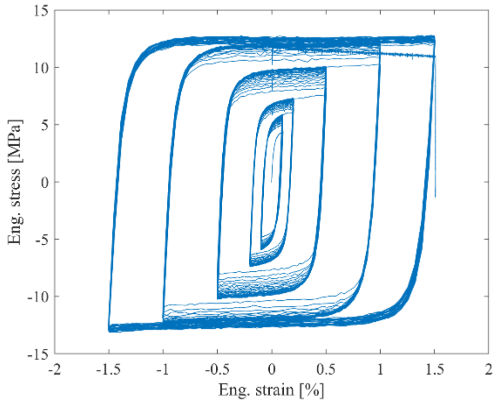

Test 3 (10^{-1} s^{-1}, 20°C)

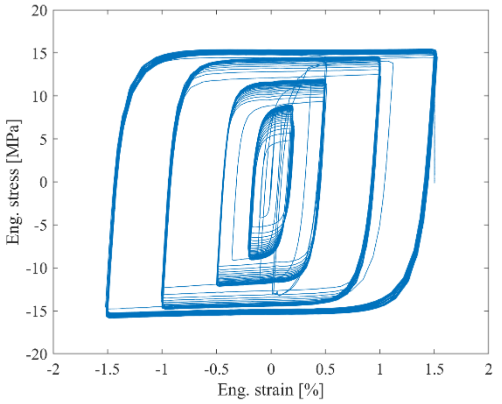

Test 4 (10^{-1} s^{-1}, 20°C)

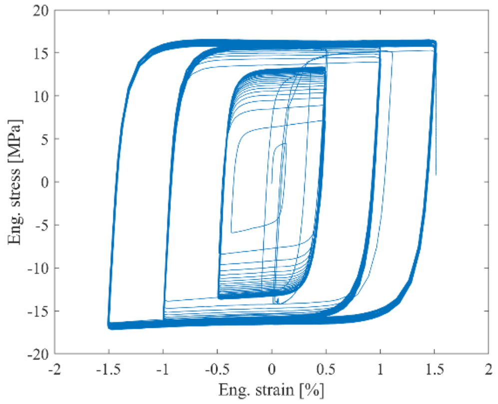

Test 5 (10^{-2} s^{-1}, 20°C)

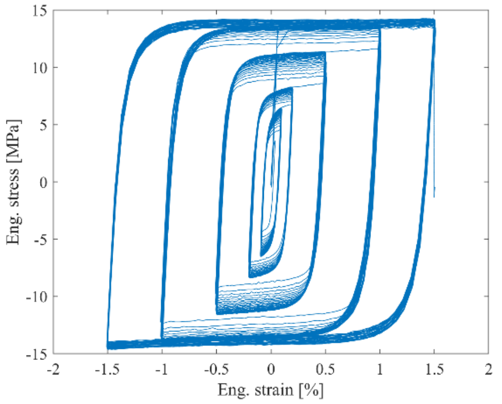

Test 6 (10^{-1} s^{-1}, 20°C)

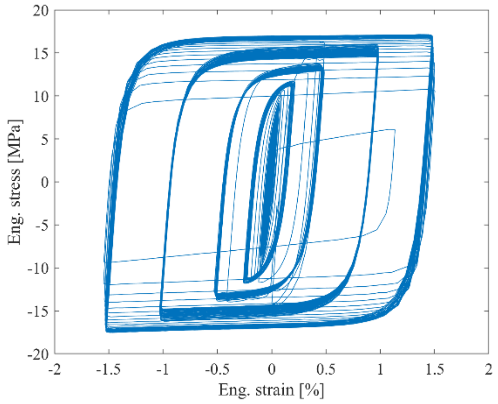

Appendix B

High temperature tests data

Test 1T (10^{-2} s^{-1}, 90°C)

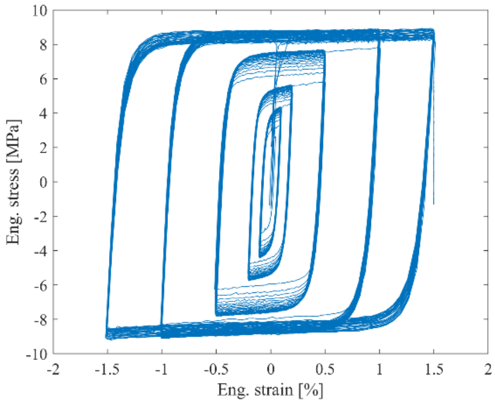

Test 2T (10^{-2} s^{-1}, 150°C)

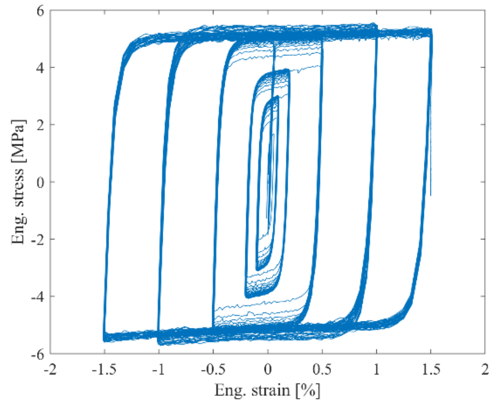

Test 3T (10^{-1} s^{-1}, 90°C)

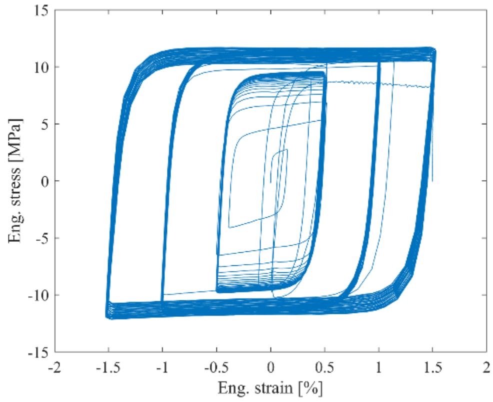

Test 4T (10^{-1} s^{-1}, 150°C)